Available online at www.sciencedirect.com
SCIENCE DIRECT®
Journal of Solid State Chemistry 178 (2005) 1559–1568
JOURNAL OF SOLID STATE CHEMISTRY
www.elsevier.com/locate/jssc

Synthesis, crystal chemistry and physical properties of the Ruddlesden–Popper phases $Sr_3Fe_{2-x}Ni_xO_{7-\delta}$ ($0 \leqslant x \leqslant 1.0$)

Liliana Mogni[a], Fernando Prado[a,*], Hugo Ascolani[a], Miguel Abbate[b], Mario S. Moreno[a], Arumugam Manthiram[c], Alberto Caneiro[a]

[a]*Centro Atómico Bariloche, CNEA, Av. E. Bustillo 9,500, 8400 San Carlos de Bariloche, Argentina*
[b]*Departamento de Física, Universidade Federal do Parana, Caixa Postal 19091, 81531-990 Curitiba PR, Brazil*
[c]*Materials Science and Engineering Program, The University of Texas at Austin, Austin, TX 78712, USA*

Received 16 November 2004; received in revised form 15 February 2005; accepted 25 February 2005

Abstract

The crystal chemistry, electronic structure, and electrical and magnetic properties of the novel perovskite-related nickel oxides $Sr_3Fe_{2-x}Ni_xO_{7-\delta}$ with $0 \leqslant x \leqslant 1.0$ have been studied. X-ray diffraction and selected area electron diffraction (ED) data indicate that the samples have a tetragonal (Space group $I4/mmm$) structure. ED patterns and high-resolution images reveal the presence of a regular stacking along the c-axis for the $x = 1.0$ sample. The lattice parameters, oxygen content, and average oxidation state of iron and nickel decrease with increasing Ni content. The electronic structure of the $x = 1.0$ sample was studied by M $2p$ X-ray photoelectron spectroscopy (XPS). An analysis of the spectra using the cluster model indicates that this material is in the negative charge-transfer regime and the ground state is dominated by the $3d^{n+1}L$ configuration with $2p$ holes (L) in the oxygen band. The insulator states are stabilized due to a p–p type band gap that arises because the p–d transfer integral T_σ dominates over the O $2p$ bandwith. Although magnetic measurements reveal the presence of ferromagnetic interactions that lead to magnetic frustration at $T \leqslant 40$ K, no long-range magnetic order was observed for the samples with $x \geqslant 0.3$. The electrical resistivity decreases with increasing Ni content as the p–p band gap tend to close due to the reduction of the T_σ value. Negative magnetoresistance ($\sim -24\%$ for $x = 0.6$ and -7% for $x = 1.0$ at 20 K and 9 T) was observed for the Ni containing samples.

Keywords: $Sr_3Fe_{2-x}Ni_xO_{7-\delta}$ oxides; Ruddlesden–Popper phases; Crystal chemistry; Electronic structure; Magnetic and electrical properties; Magnetoresistance

1. Introduction

Transition metal oxides having the perovskite or perovskite-related intergrowth structures have been extensively studied in the past years due to their remarkable electrical and magnetic properties. High-T_c superconductivity has been discovered in the layered compound $La_{2-x}Ba_xCuO_4$ [1] with a perovskite-related structure, while colossal magnetoresistance (MR) and mixed conductivity with high ionic conductivity values ($\sigma_i \approx 1\,S\,cm^{-1}$ at $T > 800\,^\circ C$) have been reported for the perovskite phases $La_{1-x}Ca_xMnO_3$ [2,3] and $La_{1-x}SrFe_{1-y}Co_yO_{3-\delta}$ [4], respectively. The search for new materials with colossal MR or mixed conductivity has prompted the exploration of layered compounds belonging to the Ruddlesden–Popper (R–P) series $A_{n+1}B_nO_{3n+1}$ with $n = 1$, 2 and 3 [5] and $A =$ La and Sr and $B =$ Mn, Fe, Co, and Ni [6–10]. Thus, large negative MR has been reported in $(La,Sr)_3Mn_2O_7$ [6] and $Sr_3(Fe,Co)_2O_7$ [7] compounds, while mixed conducting properties have been studied in the strontium iron oxides $Sr_{n+1}Fe_nO_{3n+1}$ with $n = 2$ and 3, in which Sr^{2+} was partially substituted by La^{3+} and $Fe^{3+/4+}$ by $Co^{3+/4+}$ [8–10].

*Corresponding author. fax: +54 2944 445299.
E-mail address: fprado@cab.cnea.gov.ar (F. Prado).

0022-4596/$ - see front matter © 2005 Elsevier Inc. All rights reserved.
doi:10.1016/j.jssc.2005.02.018

The crystal structure of the RP series $Sr_{n+1}Fe_nO_{3n+1}$ can be described as having layers stacked along the *c*-axis with *n* $SrFeO_3$ perovskite layers alternating with SrO rock-salt layer (see Fig. 1). The crystal structure of the $n = 2$ member $Sr_3Fe_2O_7$ is tetragonal with the space group $I4/mmm$ [11,12]. Electrical conductivity (σ) data obtained in air ($pO_2 = 0.209$ atm) show a thermally activated behavior for temperatures below $T \approx 400\,^{\circ}C$, while at temperatures above $T \approx 400\,^{\circ}C$, oxygen atoms are removed from the crystal structure, resulting in a decrease in the charge carrier concentration and σ values [8]. The partial substitution of $Fe^{3+/4+}$ by $Co^{3+/4+}$ does not modify the crystal structure and was found to improve the electrical conductivity several orders of magnitude [13,14]. The oxide-ion conductivity was also improved leading to higher oxygen permeation flux values [8].

Following the trend, it is expected that the partial substitution of Fe by Ni may increase further the oxygen non-stoichiometry of the $Sr_3Fe_2O_7$ phase due to the difficulty of stabilizing the $Ni^{3+/4+}$ oxidation state and thereby enhance the ionic conductivity σ_i of these mixed conductors. In addition, it is expected that a larger covalency of the *B*(3*d*)–O(2*p*) bond caused by the substitution of Fe by Ni will also improve the electrical conductivity of these perovskite related compounds. The Ni containing R–P phases form the series $A_{n+1}Ni_nO_{3n+1}$ (A = lanthanide or alkaline earth and $n = 1, 2, 3$ and ∞) [15,16] with a formal oxidation state of $2+/3+$ for Ni ions in these compounds. Although, the unusual mixed valent state $Ni^{3+/4+}$ is obtained in the $La_{2-x}Sr_xNiO_4$ phases with $x > 1$ [15], no R–P phases with $n = 1$, 2, and 3 and containing only Sr in the *A* site and Ni with formal oxidation state of $Ni^{3+/4+}$ in the *B* site have been reported.

In our search for new oxides with mixed conductivity we have succeed in synthesizing Ni rich oxides belonging to the $n = 2$ RP phases. In this paper we report the synthesis, crystal chemistry, and electrical and magnetic properties of the novel system $Sr_3Fe_{2-x}Ni_xO_{7-\delta}$ with $0 \leqslant x \leqslant 1.0$. Furthermore, the crystal and electronic structure of the sample with the higher Ni content ($x = 1.0$) have been studied by ED and X-ray photoelectron spectroscopy (XPS), respectively.

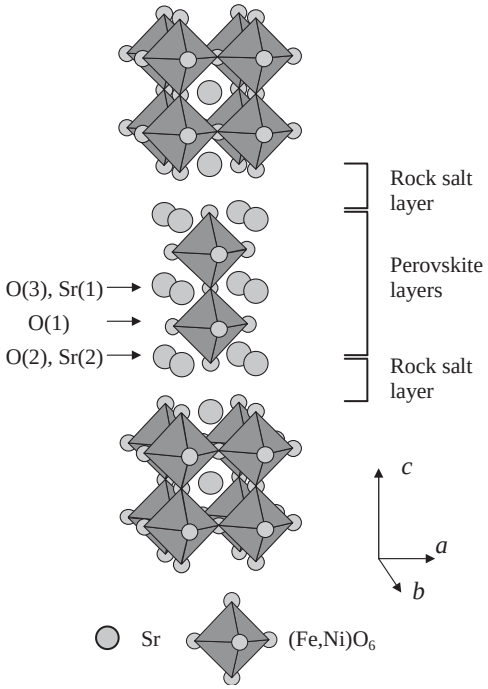

Fig. 1. Crystal structure of $Sr_3Fe_2O_7$.

2. Experimental

The $Sr_3Fe_{2-x}Ni_xO_{7-\delta}$ samples with $0 \leqslant x \leqslant 1$ were prepared by an acetic acid-based gel route. Raw materials were $SrCO_3$ (99.99%), $Fe(CH_3COO)_2$ (99%) and $Ni(CH_3COO)_2 \cdot xH_2O$ (99%+); the water content in the acetates was determined by TGA prior to the synthesis. Stoichiometric amounts of the raw materials were weighed and dissolved in acetic acid and refluxed at $T \approx 80\,^{\circ}C$ for 2 h. Small amounts of H_2O and H_2O_2 were added and the solution was refluxed further at the same temperature until a clear solution was obtained. The solution was then heated on a hot plate to obtain a greenish transparent gel. The resulting gel was dried, decomposed at $T \sim 400\,^{\circ}C$ and calcinated at 900 °C in air for 24 h. The powder was pressed into 12.7 mm discs and fired at 1300 °C under flowing oxygen for a period of 24 h. The samples were cooled to room temperature at a rate of 1 °C/min with an intermediate annealing at 400 °C for 6 h to increase the oxygen content of the phase. The oxygen content of the samples and the average oxidation state of (Fe/Ni) were inferred from iodometric titration [17].

Similar to the $Sr_3Fe_{2-x}Co_xO_{7-\delta}$ samples [13], the $Sr_3Fe_{2-x}Ni_xO_{7-\delta}$ samples were found to be unstable in ambient air at room temperature. It was found that the kinetics of degradation depends on the sample preparation method. Samples prepared by the acetic acid-based gel route were found to be more stable than those prepared by solid-state reactions. The $Sr_3Fe_{2-x}Ni_xO_{7-\delta}$ samples were stored in vacuum immediately after synthesis to prevent such degradation. The quality of the samples was verified by X-ray diffraction before and after each measurement experiment.

Powder X-ray diffraction data of the samples for Rietveld analysis were collected in the 2θ region $10 \leqslant 2\theta \leqslant 90^{\circ}$ on a Philips PW1700 diffractometer using Cu$K\alpha$ radiation and a graphite monochromator with a step of 0.02 ° per 10 s. Microanalysis of the samples were

carried out on a Philips 515 SEM microscope fitted with an EDAX 9900 energy dispersive spectrometer (EDS).

High-resolution electron microscopy and ED were carried out at room temperature on a Philips CM200 microscope operated at 200 kV. The specimens were prepared by crushing the samples in air without the use of a liquid medium and dropping them into a holey carbon film.

Fe and Ni 2*p* X-ray photoelectron spectra were recorded using a commercial VG ESCA system. The mean probing depth of the Fe and Ni 2*p* XPS is about 20 Å, which is enough to sample several atomic layers, providing information on the bulk of the material. The base pressure in the experimental chamber was in the 10^{-10} m Bar range. The spectra were collected using Al*K*α radiation and the overall energy resolution was about 1.0 eV. The energy scale was calibrated using the peak positions from the system database. The sample was scraped with a diamond file to remove surface contamination. The spectrum was normalized to the maximum intensity after a constant background subtraction.

Magnetic susceptibility measurements in the temperature range $300 \leqslant T \leqslant 570$ K were carried out with a Faraday balance magnetometer. At low temperatures ($6 \leqslant T \leqslant 300$ K), the variations of the magnetic susceptibility with temperature under zero-field-cooled (ZFC) and field cooled (FC) conditions and with applied field at several temperatures were recorded with a vibrating sample magnetomer (VSM).

Conductivity measurements as a function of temperature were carried out by a standard four-probe method on bar shaped samples in the 5–300 K temperature range under applied magnetic fields between 0 and 9 T. The electrical wires were attached to the sample using Ag paste on sputtered gold contacts.

3. Results and discussion

3.1. Crystal structure and oxygen content

Fig. 2 shows the X-ray powder diffraction patterns of the $Sr_3Fe_{2-x}Ni_xO_{7-\delta}$ samples for $0 \leqslant x \leqslant 1.0$. The inspection of the XRD patterns indicates that the crystal structure of the Ni doped samples is isotypic with the crystal structure of the parent compound $Sr_3Fe_2O_{7-\delta}$. No secondary phases were detected in the $Sr_3Fe_{2-x}Ni_xO_{7-\delta}$ samples. However, XRD patterns reveal large preferred orientation in the [001] direction, which is evident in the $x = 0$ and 0.6 samples at the (006) and (00$\underline{10}$) reflections (see Fig. 2). SEM observations and microanalysis on the $Sr_3Fe_{2-x}Ni_xO_{7-\delta}$ samples confirmed the absence of secondary phases and a homogeneous distribution of Ni in the ceramic grains.

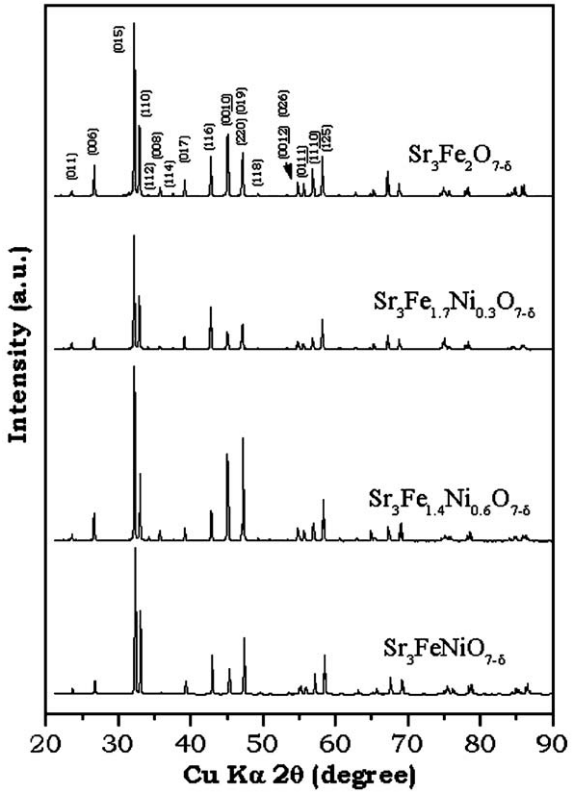

Fig. 2. X-ray powder diffraction patterns of the $Sr_3Fe_{2-x}Ni_xO_{7-\delta}$ samples. Miller indices of some representative reflections are given.

Table 1
Oxygen content, oxidation state, lattice parameters, and unit cell volume of $Sr_3Fe_{2-x}Ni_xO_{7-\delta}$

x	Oxygen content, $7-\delta$	Oxidation state of (Fe,Ni)	a (Å)	c (Å)	V (Å^3)
0	6.76 (1)	3.76	3.8678 (1)	20.174 (1)	301.79
0.3	6.66 (4)	3.66	3.8618 (1)	20.162 (1)	300.68
0.6	6.64 (4)	3.64	3.8510 (1)	20.139 (1)	298.66
1.0	6.63 (1)	3.63	3.8415 (1)	20.040 (1)	295.73

The lattice parameters of the $Sr_3Fe_{2-x}Ni_xO_{7-\delta}$ phases were refined by the Rietveld method on the basis of the tetragonal space group *I*4/*mmm*, and the values are given in Table 1. The lattice parameters a and c and the unit cell volume V decrease with increasing Ni content. For the $x = 0$ sample, the refined lattice constant c is slightly higher than the value obtained from XRD data by Dann et al. [11]. The analysis of XPS data of $Sr_3Fe_2O_{7-\delta}$ [18] and $Sr_3FeNiO_{7-\delta}$ (see Section 3.2 and references therein) using cluster model calculations indicates that Fe ions are in the high spin state, while Ni ions are in the low spin state. Thus, the variation of the unit cell volume with increasing Ni content is due to

the smaller ionic radii of Ni^{3+} ($r_{vi} = 0.56$ Å) and eventually Ni^{4+} ($r_{vi} = 0.48$ Å) in the low spin state compared to the ionic radii of Fe^{3+} ($r_{vi} = 0.645$ Å) and Fe^{4+} ($r_{vi} = 0.585$ Å) in the high spin state [19]. During the refinement, the oxygen content values were fixed to the values obtained by iodometric titration.

Considering that the mixed occupancy by Ni and Fe of the same crystallographic site combined with the oxygen deficiency can gives place to different microstructural arrangements we paid attention to the presence of extra reflections or diffuse intensity distributions in the ED patterns since diffuse intensities are usually associated with some type of disorder in the lattice. The inspection at room temperature of the reciprocal space of the $x = 1.0$ sample by selected area electron diffraction (SAED) revealed only reflections consistent with the $I4/mmm$ space group. In Fig. 3 are shown representative [010] and [001] zone-axis ED patterns of $Sr_3FeNiO_{7-\delta}$. The absence of any other features in the ED patterns should be noticed. This means that in this sample there is a highly regular stacking along the c-axis and there is no extra long-range ordering. One example of such regularity is provided by the high-resolution image along the [010] zone axis shown in Fig. 4.

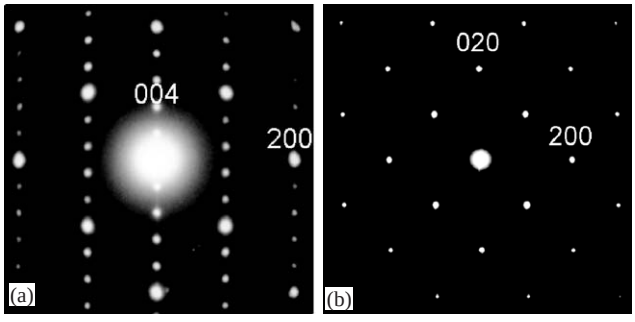

Fig. 3. (a) [010] and (b) [001] SAED zone-axis patterns.

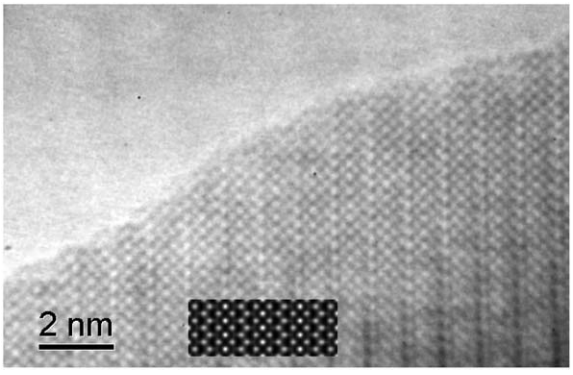

Fig. 4. [010] HREM of $Sr_3FeNiO_{7-\delta}$. Superimposed is the simulated image obtained with defocus close to −33 nm and crystal thickness of 20 Å.

The oxygen content of the $Sr_3Fe_{2-x}Ni_xO_{7-\delta}$ compounds was determined by iodometric titration and the results are given in Table 1. All the samples exhibit oxygen non-stoichiometry caused by the difficulty of stabilizing Ni^{4+}. The oxygen deficiency of the oxygen-annealed samples is seen to be higher in the Ni-doped samples ($\delta \sim 0.35$) compared to that in both the $Sr_3FeO_{7-\delta}$ sample and the $Sr_3Fe_{2-x}Co_xO_{7-\delta}$ compounds ($\delta \sim 0.2-0.3$) [13,20]. This trend indicates that the difficulty of stabilizing the formal oxidation state $4+$ increases ongoing from Fe to Ni. In spite of this, the oxygen content value $7-\delta = 6.63(1)$ obtained by iodometric titration for the $x = 1.0$ sample suggests that the average oxidation state of Ni could be higher than $3+$ if an oxidation state of $4+$ is assigned to Fe according to XPS data (see Section 3.2). The oxygen content value obtained by iodometric titration for the $x = 1.0$ sample was verified using TGA by reducing the sample in dry H_2 at high temperature; it gave a value $7-\delta = 6.62$ (1), which is in excellent agreement with the value obtained by iodometry. Nevertheless, it would be desirable to study the $x = 1.0$ sample by Mössbauer spectroscopy for obtaining unambiguously the Fe oxidation state and therefore the corresponding oxidation state of Ni ions.

3.2. Electronic structure

Fig. 5 shows the Fe $2p$ XPS spectrum of the $Sr_3FeNiO_{7-\delta}$ compound. The spectrum is in agreement with the previous reports for the related Fe^{4+} material $SrFeO_3$ [21]. The Fe $2p$ spectrum is split by the Fe $2p$ spin–orbit effect into the $2p_{3/2}$ and $2p_{1/2}$ regions. The main $2p_{3/2}$ peak around 710 eV is followed by a distinct satellite around 718 eV. The main peak corresponds to the well-screened $2p^5 3d^6 L$ final state configuration, while the satellite corresponds to the poorly screened $2p^5 3d^5$ final state configuration (where L denotes a $2p$ hole in the oxygen band) [22,23].

Fig. 5 also compares the experimental and calculated Fe $2p$ spectra of $Sr_3FeNiO_{7-\delta}$ (the calculation was mounted on the corresponding Shirley-type background). The satellites in the Fe $2p$ XPS spectra were analyzed using cluster model calculations [22]. The cluster model is solved using the configuration interaction method. The parameters of the model are the charge-transfer energy Δ, the Coulomb repulsion U, the core-hole potential Q, and the p–d transfer integral T_σ [23]. The ground and final states are expanded in terms of charge-transfer configurations, and the core-level transitions are calculated within the sudden approximation.

The calculation reproduces the energy separation and relative intensity of the satellite. The parameters for Fe are $\Delta = 0$ eV, $U = 7.5$ eV, $Q = 8.4$ eV, and $T_\sigma = 2.2$ eV [24]. The symmetry of the ground state (^5E) is dictated

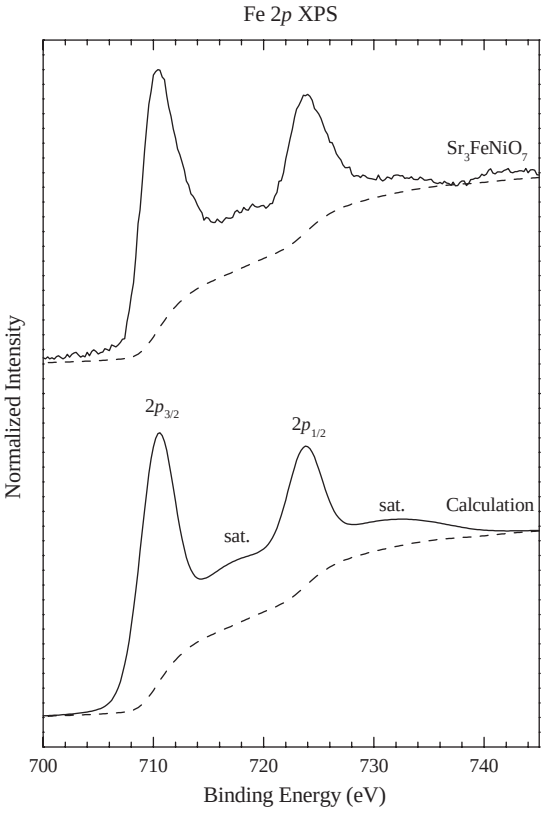

Fig. 5. Fe 2*p* X-ray photoelectron (XPS) spectrum of $Sr_3FeNiO_{7-\delta}$ compared to the cluster model calculation.

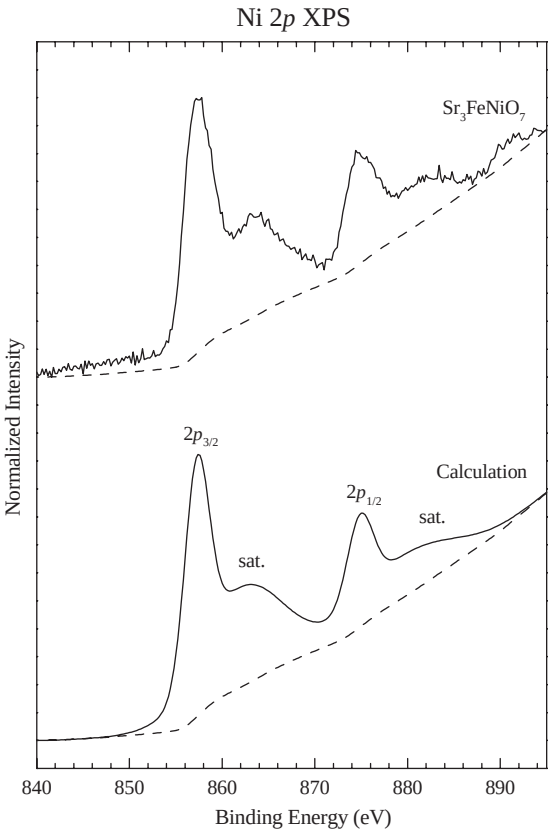

Fig. 6. Ni 2*p* X-ray photoelectron (XPS) spectrum of $Sr_3FeNiO_{7-\delta}$ compared to the cluster model calculation.

by the base $3d^4$ configuration ($t_{2g}{}^3e_g{}^1$) [24]. The occupations of the different configurations in the ground state are: 36% $3d^4$, 58% $3d^5L$ and 6% $3d^6L^2$ [24].

Fig. 6 shows the Ni 2*p* XPS spectrum of the $Sr_3FeNiO_{7-\delta}$ compound. The spectrum is in agreement with the previous reports for the related Ni^{3+} material $PrNiO_3$ [25]. The calculation reproduces the energy separation and relative intensity of the satellite. The parameters for Ni are $\Delta = 1\,\text{eV}$, $U = 7\,\text{eV}$, $Q = 9\,\text{eV}$, and $T_\sigma = 1.8\,\text{eV}$ [26]. The symmetry of the ground state (^2E) follows from the original $3d^7$ configuration ($t_{2g}{}^6e_g{}^1$) [26]. The occupations of the different configurations in the ground state are: 28% $3d^7$, 60% $3d^8L$ and 10% $3d^9L^2$ [26].

The occupation of the $3d^{n+1}L$ configuration in $Sr_3FeNiO_{7-\delta}$ is larger than that of the $3d^n$ configuration. This means that the ground state is dominated by O 2*p* holes giving a negative charge-transfer regime [27]. This configuration is actually a continuum and should lead to a metallic ground state. The band gap of $Sr_3Fe_{2-x}Ni_xO_{7-\delta}$ appears because T_σ is larger than the bandwidth W [27]. The lowest lying excitations in these cases are $3d^{n+1}L + 3d^{n+1}L \rightarrow 3d^{n+1} + 3d^{n+1}L^2$. These charge fluctuations involve O 2*p* holes and consequently the band gap is of the *p–p* type [27].

3.3. Magnetic properties

Fig. 7 shows the variation of the molar magnetic susceptibility χ_{mol} with temperature for the $Sr_3Fe_{2-x}Ni_xO_{7-\delta}$ samples with $0.3 \leqslant x \leqslant 1.0$. The measurements were carried out under ZFC and FC conditions with an applied magnetic field of 100 G. The χ_{mol} vs. T curves exhibit a paramagnetic behavior and a lack of long-range magnetic order at temperatures above $T \sim 40\,\text{K}$. At $T \sim 40\,\text{K}$, the ZFC molar susceptibility curves exhibit a maximum and deviation from the FC molar susceptibility curves that show no or slight variation with temperature in the range $5 \leqslant T \leqslant 40\,\text{K}$. This behavior is usually due to a magnetic frustration that leads to a spin-glass or cluster-glass behavior. The blocking temperature of this spin/cluster-glass behavior, revealed by the maximum of the ZFC curve, slightly changes from $T_B = 40\,\text{K}$ for the samples with $x = 0.3$ and 0.6 to $T_B = 33\,\text{K}$ for the sample with $x = 1.0$.

The field dependence of the magnetization for the sample $x = 1.0$ at various temperatures is shown in Fig. 8. For $T = 100$ and 200 K, the magnetization M increases linearly with the field H, which is typical for a paramagnetic system. At $T = 40\,\text{K}$, the M vs. H plot exhibit a very small curvature, while at temperatures below $T = 40\,\text{K}$, where the χ_m vs. T plots reveal a

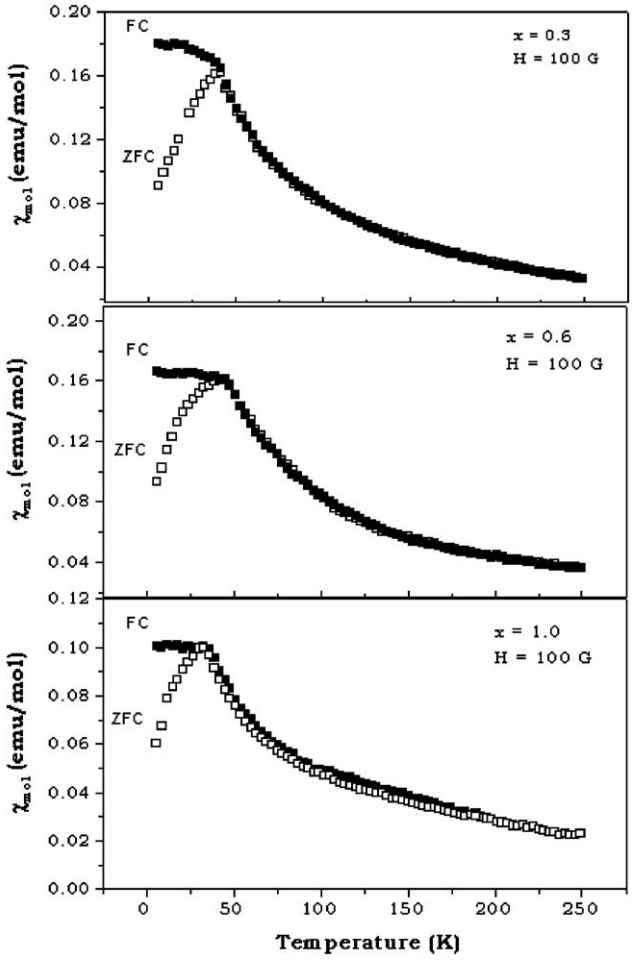

Fig. 7. Variations of the molar magnetic susceptibility of the oxygen-annealed $Sr_3Fe_{2-x}Ni_xO_{7-\delta}$ samples with temperature under an applied field of 100 G: (a) $x = 0.3$, (b) $x = 0.6$, and (c) $x = 1.0$. Solid and open symbols refer, respectively, to field-cooled (FC) and zero-field-cooled (ZFC) data.

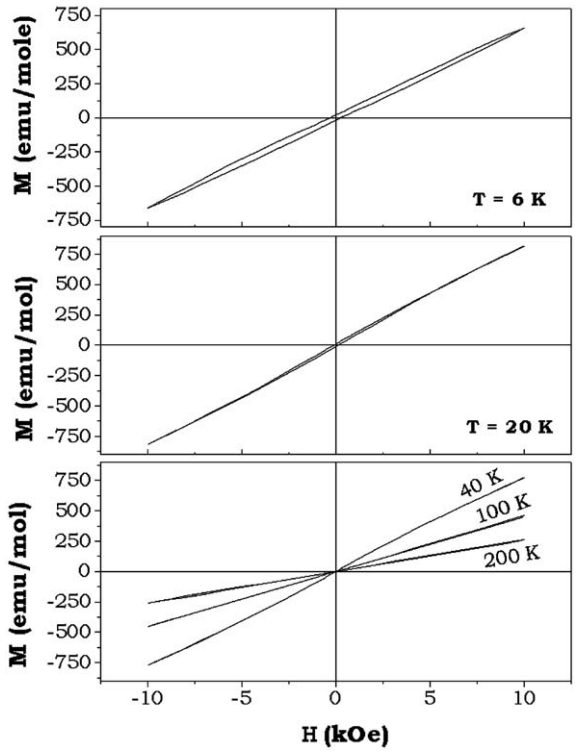

Fig. 8. Variations of the magnetization with the applied field of $Sr_3FeNiO_{7-\delta}$ ($x = 1.0$) at various temperatures.

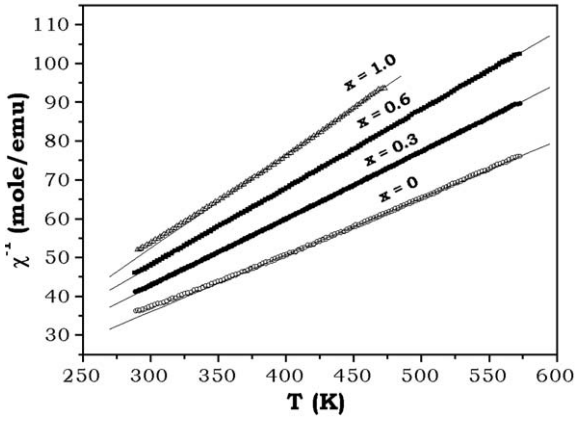

Fig. 9. Variations of the inverse molar magnetic susceptibility of the $Sr_3Fe_{2-x}Ni_xO_{7-\delta}$ samples. The straight line corresponds to the linear extrapolation of the data for $T \geqslant 350$ K.

spin/cluster glass behavior, narrow hysteresis loops show up.

The effective magnetic moment μ_{eff} per (Fe,Ni) atom and the Weiss constant θ were determined from magnetic susceptibility measurements obtained in the temperature range $300 \leqslant T \leqslant 570$ K under a magnetic field $H = 5000\,G$ using a Faraday balance magnetometer. The measurements were performed in poor vacuum ($P = 1.3 \times 10^{-3}$ atm). Each sample was heated at a rate of 1 °C/min and then cooled down to room temperature at the same rate. Special care was taken to prevent the reduction of the samples at high temperature. Thus, the maximum temperature for the measurements was fixed at 570 K. The magnetization values at room temperature were reproducible after heating and cooling indicating that no changes were induced in the chemical compositions of the samples.

Fig. 9 shows the variations of the inverse molar magnetic susceptibility with temperature for the $Sr_3Fe_{2-x}Ni_xO_{7-\delta}$ samples with $0 \leqslant x \leqslant 1.0$ in the paramagnetic region $300 \leqslant T \leqslant 570$ K. The $\chi^{-1}(T)$ data exhibit little deviations from the Curie–Weiss law $\chi(T) = C/(T - \theta)$. The magnetic constants C and θ were determined from the linear extrapolation of the $\chi^{-1}(T)$ data obtained at $T \geqslant 350$ K. The values of the magnetic parameters obtained from the $\chi^{-1}(T)$ data are listed in Table 2. The θ values obtained for $Sr_3Fe_{2-x}Ni_xO_{7-\delta}$ vary from 45 K for the $x = 0$ sample to 82 K for the $x = 1.0$ sample. The positive values of θ even in the $x = 0$ sample indicate the presence of

Table 2
Magnetic data of $Sr_3Fe_{2-x}Ni_xO_{7-\delta}$ giving the values of temperature range (T_{range}), Curie constant (C), Weiss constant (θ), experimental effective magnetic moment (μ_{eff}), and calculated spin-only magnetic moment (μ_{theo})[a]

x	T_{range} (K)	C (emu K/mol)	θ (K)	μ_{eff} (μ_B)	μ_{theo}(μ_B)
0	350–470	6.82	54	5.24	5.15
0.3	350–570	5.76	55	4.82	4.79
0.6	350–570	4.96	64	4.47	4.28
1.0	350–570	4.16	83	4.09	3.61

[a]See Table 1 for the oxygen content values of the samples.

ferromagnetic interactions in the $Sr_3Fe_{2-x}Ni_xO_{7-\delta}$ system that are reinforced with the presence of nickel in the crystal structure. In the case of the $x = 0$ sample, the value $\theta \sim 45$ K is in disagreement with our previous result [13] where a negative value of θ was reported in agreement with antiferromagnetic correlations. Discrepancies arise from the temperature range used to determine the magnetic constants and the oxygen content of the samples. In this work the temperature range is well above room temperature, which allows a better determination of the magnetic constants values compared to the previous work [13]. A positive value $\theta \sim 60$ K implying the presence of ferromagnetic interactions was also obtained by Adler [28] for $Sr_3Fe_2O_{7-\delta}$ annealed at oxygen pressures of 60 MPa. The effective magnetic moments per (Fe/Ni) site were obtained using the relation $\mu_{eff} = 2.84 \times \sqrt{C/2}$. The slope ($C^{-1}$) of the $\chi^{-1}(T)$ data increases with increasing Ni content in the samples, leading to a decrease in μ_{eff}. This behavior is expected as a consequence of the substitution of Fe^{3+} ($t_{2g}^3 e_g^2$) ($S = 5/2$) and Fe^{4+} ($t_{2g}^3 e_g^1$) ($S = 2$) ions in the high spin state by Ni^{3+} ($t_{2g}^6 e_g^1$) ($S = 1/2$) and eventually Ni^{4+} ($t_{2g}^6 e_g^0$) ($S = 0$) ions in the low spin state, whose spin-only magnetic moments are lower than those of the $Fe^{3+/4+}$ ions. The experimental values of μ_{eff} are compared in Table 2 with the magnetic moments (μ_{theo}) calculated from the spin-only magnetic moments of the transition metal ions using the relation,

$$\mu_{theo} = \sqrt{\sum_i f_i \times \mu_{s,i}^2} \quad (1)$$

where f_i and $\mu_{s,i}$ represent the fraction and the spin-only magnetic moment of the transition metal ion i, respectively. The calculations were carried out assuming the presence of high spin $Fe^{3+/4+}$ and low spin Ni^{3+} for the $x = 0$, 0.3 and 0.6 samples. The fractions of Fe ions in the 3+ and 4+ oxidation states were estimated from the oxygen content values of the samples listed in Table 1. The experimental μ_{eff} values are in excellent agreement with the calculated values of μ_{theo} for the $x = 0$ and 0.3 samples and in fair agreement for the $x = 0.6$ sample (see Table 2). In the case of the sample with $x = 1.0$, we have assumed that the Fe ions are in the 4+ oxidation state while the Ni ions are in both the 3+ and the 4+ oxidation state. The fraction of Ni ions in the 3+ oxidation state is 0.7 and is obtained from the oxygen content value of the sample. In spite of the good agreement between the calculated and experimental values, a progressive deviation of μ_{theo} values from μ_{eff} is observed on going from $x = 0.3$ to 1.0. The assumptions on the Fe and Ni oxidation states to calculate μ_{theo} are based on the analysis of XPS data (see Section 3.2 and Ref. [18]). To corroborate these results, more precise information about the Fe and Ni oxidation states in the $Sr_3Fe_{2-x}Ni_xO_{7-\delta}$ compounds using Mössbauer spectroscopy would be needed.

3.4. Electrical resistivity and magnetoresistance

The variations of the electrical resistivity (ρ) with temperature of the $Sr_3Fe_{2-x}Ni_xO_{7-\delta}$ phases with $0.0 \leqslant x \leqslant 1.0$ are shown in Fig. 10 in the temperature range $5 \leqslant T \leqslant 300$ K. The parent compound $Sr_3Fe_2O_{7-\delta}$ annealed in pure oxygen exhibits a semiconducting behavior ($d\rho/dT < 0$). The plot shows a reasonable agreement with the data previously reported for $Sr_3Fe_2O_{7-\delta}$ [13]. At room temperature, ρ varies between 0.1 and 10 Ω cm depending on the oxygen content of the $Sr_3Fe_2O_{7-\delta}$ phase. As the temperature decreases, ρ increases reaching values as high as 10^6 and 10^7 Ω cm at $T < 100$ K. The replacement of Fe by Ni causes a remarkable decrease by several orders of magnitude in the electrical resistivity at low temperatures. The inset in Fig. 10 shows the Arrhenius plot of the variation of the electrical resistivity with inverse temperature for the $Sr_3Fe_{2-x}Ni_xO_{7-\delta}$ phases. It is evident from the shape of

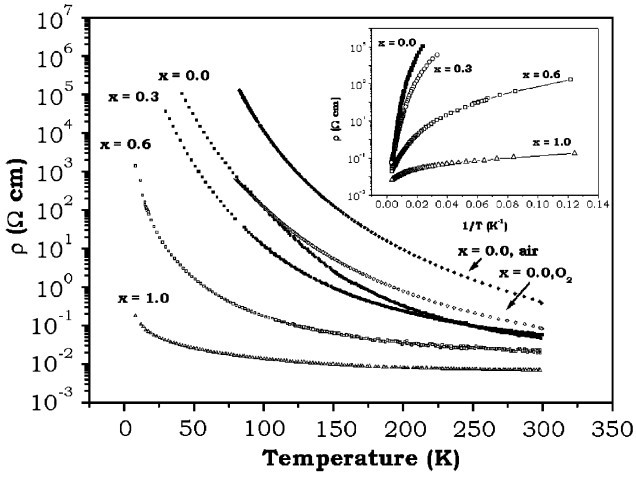

Fig. 10. Variations of resistivity with temperature for the oxygen-annealed $Sr_3Fe_{2-x}Ni_xO_{7-\delta}$ samples ($0.0 \leqslant x \leqslant 1.0$). ρ vs. T curves of $Sr_3Fe_2O_{7-\delta}$ reported in Ref. [13] for samples annealed in air (◆) and oxygen (◇) are also included. The inset shows the Arrhenius plot for the electrical resistivity.

the curves that the activation energy of the electrical transport process changes with temperature and decreases as the Ni content increases. The analysis of the electrical resistivity data using the relation $\rho = \rho_0 \exp(T/T_0)^{1/n}$ does not show clear evidence that the Ni-doped samples behave like a disordered system with electronic states localized close to the Fermi level ($n = 4$) as was reported for the $Sr_3Fe_{2-x}Co_xO_{7-\delta}$ system [13,20]. Adler et al. [29] have induced an insulator–metal transition in $Sr_3Fe_2O_{7-\delta}$ by increasing the pressure. Although metallic behavior could not be obtained, the substitution of Co for Fe also reduces several orders of magnitude at low temperatures the resistivity of the $Sr_3Fe_{2-x}Co_xO_{7-\delta}$ compounds on going from $x = 0$ to 0.8 [13,14,20]. To explain the effect of the high pressure and the substitution of Fe by Co on the resistivity, it was argued that both effects strength the covalent interaction in $M(3d)$–$O(2p)$–$M(3d)$ and thereby increase the bandwidth of the conduction band, causing a closure of the band gap [13,14,29]. More recently, XPS data of the $Sr_3Fe_2O_{7-\delta}$ compound have shown that the band-gap arises because the p–d transfer integral $T_\sigma = 2.2$ eV dominates over the O $2p$ bandwidth [18,27]. An analysis of the XPS data of the sample with a Ni content $x = 1.0$ (Section 3.2) indicates that the p–d transfer integral $T_\sigma = 1.8$ eV is clearly smaller than the T_σ value obtained for the $Sr_3Fe_2O_{7-\delta}$ phase, leading to a smaller band gap and higher electrical conductivity as the Ni content increases. The substitution of Fe by Ni atoms also leads to a reduction of the M–O distances, causing an increase in the O $2p$ bandwidth and consequently a reduction in the electrical resistivity. However, the reduction in the unit cell volume due to the substitution of Fe by Ni is small (~2%) compared to the volume change caused by pressure on $Sr_3Fe_2O_{7-\delta}$ to obtain the transition to the metallic state (~11% at 20 GPa) [29]. Thus, although both effects cause a decrease in the electrical resistivity as the Ni content increases, the reduction of the p–p band gap due to the smaller p–d transfer T_σ value is the main contribution to explain the decrease in the electrical resistivity value with the Ni content.

The transport properties of the $Sr_3Fe_{2-x}Ni_xO_{7-\delta}$ compounds were further investigated by measuring the effects of an applied field (H) on the electrical resistivity (ρ). Fig. 11 shows the variations of ρ with the applied field H in the range $0 \leqslant H \leqslant 9$ T at different fixed temperatures ($T = 20$, 40, 60 and 100 K) for the samples with $x = 0.6$ and 1.0. The samples were first cooled in zero field to $T = 20$ K. Afterwards, the $\rho(H)$ response was recorded by changing the applied field from 0 to 9 T and then from 9 to 0 T with a ramp of 0.5 T/min. Before measuring the $\rho(H)$ curve at a given temperature, the electrical resistivity was stabilized in order to minimize relaxation processes that could lead to confusing results. The $\rho(H)$ curves in both samples clearly show the

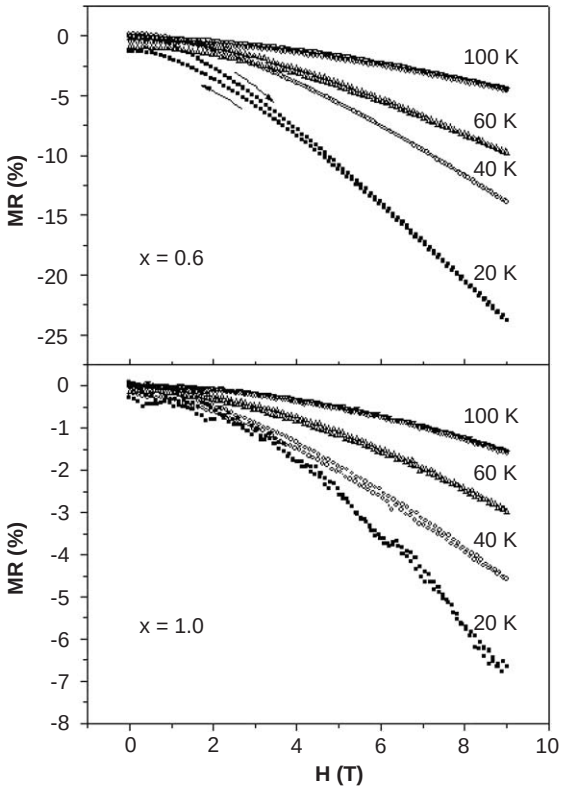

Fig. 11. Variations of the electrical resistivity ρ with the applied field at different fixed temperatures for the $Sr_3Fe_{2-x}Ni_xO_{7-\delta}$ compounds: (a) $x = 0.6$ and (b) $x = 1.0$.

presence of negative MR that decreases as the temperature increases with no evidence of saturation at high magnetic fields. The percentage of MR obtained for the $x = 0.6$ and 1.0 samples was 24% and 7%, respectively, at 20 K and can be considered as large negative MR. The MR response of the $x = 0$ sample has been reported by Ghosh and Adler [7,14] to be ~−4% at 10 K and 7 T and zero at 50 K. Therefore, we assume that the presence of Ni atoms in the perovskite layers is responsible of the negative MR detected for the $x = 0.6$ and 1.0 samples. Like the $Sr_3Fe_{2-x}Co_xO_{7-\delta}$ compounds [14], the negative MR effect of the $x = 0.6$ sample is larger than the negative MR effect measured for the $x = 1.0$ sample. Unlike other systems such as the manganites [2,3], $La_{1-x}Sr_xCoO_3$ [30,31], Sr_2FeMoO_6 [32], and layered compounds [6,7,33], where negative MR effects are correlated to ferromagnetic and metallic states, the Ni-doped samples only show some evidence of ferromagnetic interactions. For instance, the magnetic behavior of the Ni-doped samples includes magnetic frustration a $T < 40$ K as a consequence of competing antiferromagnetic and ferromagnetic interactions present in the $Sr_3Fe_{2-x}Ni_xO_{7-\delta}$ system. The M vs. H curves at T below T_B exhibit a little hysteresis that indicates ferromagnetic interactions. Finally, the parent compound $Sr_3Fe_2O_{7-\delta}$ is antiferromagnetic with

$T_N \sim 110$ K [28] since the correlation effects of the Fe–O–Fe interaction predominates over ferromagnetic interactions presents at temperatures above T_N. These ferromagnetic interactions are revealed by the positive values obtained for the magnetic constant θ of $Sr_3Fe_2O_{7-\delta}$. The substitution of Fe by Ni increases the value of θ, indicating that ferromagnetic interactions are enhanced with the addition of Ni.

The ferromagnetic interactions observed in the $Sr_3Fe_{2-x}Ni_xO_{7-\delta}$ phases suggest the formation of ferromagnetic domains that could explain the negative MR response of the $Sr_3Fe_{2-x}Ni_xO_{7-\delta}$ phases via intragranular and intergranular effects [34]. Further work is necessary to correlate the magnetic properties of the $Sr_3Fe_{2-x}Ni_xO_{7-\delta}$ phases with the magneto-transport properties.

4. Conclusion

Novel nickel oxides belonging to the $n = 2$ RP phases, $Sr_3Fe_{2-x}Ni_xO_{7-\delta}$ with $0 \leqslant x \leqslant 1.0$, were synthesized by an acetic acid-based gel route. The crystal structure of the $Sr_3Fe_{2-x}Ni_xO_{7-\delta}$ system remains tetragonal (Space group $I4/mmm$) after the substitution of Fe by Ni for the Ni content range $0 \leqslant x \leqslant 1.0$. ED patterns and high-resolution images indicate good long-range order for the $x = 1.0$ sample with no evidences of diffuse intensities suggesting structural disorder. The analysis of the XPS data of the $x = 1.0$ sample using the cluster model shows that this material is in the negative charge-transfer regime and the ground state is dominated by the $3d^{n+1}L$ configuration with $2p$ holes (L) in the oxygen band. The electronic configuration of Fe atoms was found to be high spin $3d^4$: $t_{2g}^3 e_g^1$, while Ni atoms are mainly in the low spin $3d^7$: $t_{2g}^6 e_g^1$ configuration. The insulator states are stabilized due to a p–p type band gap, which arises because the p–d transfer integral T_σ dominates over the O $2p$ bandwidth. The reduction of the electrical resistivity with the substitution of Fe by Ni is a consequence of the decrease in the T_σ value that reduces the p–p band gap. Magnetic measurements reveal the presence of ferromagnetic interactions that lead to magnetic frustration at $T \leqslant 40$ K. However, no long-range magnetic order was observed for the samples with $x \geqslant 0.3$. The effective magnetic moments calculated from the spin-only contribution, considering the electronic configurations obtained from XPS data, are in good agreement with the effective magnetic moment values obtained from the χ_m vs. T plots at $T > 300$ K. The negative MR ($\sim -24\%$ for $x = 0.6$ and -7% for $x = 1.0$ at 20 K and 9 T) observed for the Ni-containing samples was attributed to the possible formation of ferromagnetic domains suggested by the experimental evidence of ferromagnetic interactions.

Acknowledgments

We gratefully acknowledge Dr. A. Butera for magnetic measurements. This work was supported by CNEA (Argentine Research Commission), Fundación Antorchas (Argentina), ANPCyT through PICT 02-12-12455 and 03-12-14493, Cooperation Program ECOS-SUD, the Brazilian Funding Agencies CNPq, PRONEX, and Fundação Araucária, and the Welch Foundation Grant F-1254.

References

[1] J.C. Bednorz, K. Muller, Z. Phys. B 64 (1986) 189–193.
[2] R.V. Helmolt, J. Wecker, B. Holzapfel, L. Schultz, K. Samwer, Phys. Rev. Lett. 71 (1993) 2331–2333.
[3] S. Jin, T.H. Tieffel, H. McCormack, R.A. Fastnacht, R. Ramesh, L.H. Chen, Science 264 (1994) 413–415.
[4] Y. Teraoka, H.M. Zhang, S. Furukawa, N. Yamazoe, Chem. Lett. (1985) 1743–1746.
[5] S.N. Ruddlesden, P. Popper, Acta Crystallogr. 11 (1958) 54–55.
[6] Y. Moritomo, A. Asamitsu, H. Kuwahara, Y. Tokura, Nature (London) 380 (1996) 141–144.
[7] S. Ghosh, P. Adler, Solid State Commun. 116 (2000) 585–589.
[8] F. Prado, T. Armstrong, A. Caneiro, A. Manthiram, J. Electrochem. Soc. 148 (2001) J7–J14.
[9] T. Armstrong, F. Prado, A. Manthiram, Solid State Ionics 140 (2001) 89–96.
[10] A. Manthiram, F. Prado, T. Armstrong, Solid State Ionics 152–153 (2002) 647–655.
[11] S.E. Dann, M.T. Weller, D.B. Currie, J. Solid State Chem. 97 (1992) 179–185.
[12] S.E. Dann, M. T Weller, D.B. Currie, M.F. Thomas, A.D. Al-Rawwas, J. Mater. Chem. 3 (1993) 1231–1237.
[13] F. Prado, A. Manthiram, J. Solid State Chem. 158 (2001) 307–314.
[14] S. Ghosh, P. Adler, J. Mater. Chem. 12 (2002) 511–521.
[15] A. Manthiram, J.P. Tang, V. Manivannan, J. Solid State Chem. 148 (1999) 499–507.
[16] M. Greenblatt, Curr. Opin. Solid State Mater. Sci. 2 (1997) 174–183.
[17] A. Manthiram, S. Swinnea, Z.T. Sui, H. Steinfink, J.B. Goodenough, J. Am. Chem. Soc. 109 (1987) 6667–6669.
[18] M. Abbate, H. Ascolani, F. Prado, F. Caneiro, Solid State Commun. 129 (2004) 113–116.
[19] R.D. Shannon, Acta Crystallogr. A 32 (1976) 751–767.
[20] G.M. Veith, R. Chen, G. Popov, M. Croft, Y. Shokh, I. Nowik, M. Greenblatt, J. Solid State Chem. 166 (2002) 292–304.
[21] A.E. Bocquet, A. Fujimori, T. Mizokawa, T. Saitoh, H. Namatame, S. Suga, N. Kimizuka, Y. Takeda, M. Takano, Phys. Rev. B 45 (1992) 1561–1570.
[22] J. Kanamori, A. Kotani (Eds.), Core-Level Spectroscopy of Condensed Systems, Springer, Berlin, 1988.
[23] G. Van der Laan, C. Westra, C. Haas, G.A. Sawatzky, Phys. Rev. B 23 (1981) 4369–4380.
[24] M. Abbate, G. Zampieri, J. Okamoto, A. Fujimori, S. Kawasaki, M. Takano, Phys. Rev. B 65 (2002) 165120.
[25] T. Mizokawa, A. Fujimori, T. Arima, Y. Tokura, N. Mori, J. Akimitsu, Phys. Rev. B 52 (1995) 13865–13873.
[26] M. Abbate, G. Zampieri, F. Prado, A. Caneiro, J.M. Gonzalez-Calbet, M. Vallet-Regi, Phys. Rev. B. 65 (2002) 155101.

[27] T. Mizokawa, H. Namatame, A. Fujimori, K. Akeyama, H. Kondoh, H. Kuroda, N. Kosugi, Phys. Rev. Lett. 67 (1991) 1638–1641.
[28] P. Adler, J. Solid State Chem. 130 (1997) 129–139.
[29] P. Adler, U. Scwarz, K. Syassen, G.Kh. Rozenberg, G.Yu. Machavariani, A.P. Milner, M.P. Pasternak, M. Hanfland, Phys. Rev. B 60 (7) (1999) 4609–4617.
[30] G. Briceño, H. Chang, X. Sun, P.G. Schultz, X.D. Xiang, Science 270 (1995) 273–275.
[31] A. Maignan, C. Martin, N. Nguyen, B. Raveau, Solid State Sci. 3 (2001) 57–63.
[32] K.I. Kobayashi, T. Kimura, H. Sawada, K. Terakura, Y. Tokura, Nature (London) 395 (1998) 677–680.
[33] Y. Shimikawa, Y. Kubo, T. Manako, Nature (London) 379 (1996) 53–55.
[34] M. Sánchez-Andújar, J. Mira, J. Rivas, M.A. Señarís-Rodríguez, J. Magn. Magn. Mater. 263 (2003) 282–288.